Received June 1999
Revised December 1999
Accepted January 2000

Melting from heat sources flush mounted on a conducting vertical wall

Bruno Binet
Process modelling and instrumentation IMI – National Research Council of Canada, Québec, Canada
Marcel Lacroix
Département de génie mécanique, Université de Sherbrooke, Québec, Canada

Keywords *Melting, Natural convection, Numerical methods*

Abstract *A numerical study is conducted for natural convection dominated melting inside discretely heated rectangular enclosures. This study finds applications in the design and operation of thermal energy storage units and the cooling of electric equipment. Results show the benefits of discrete heating over uniform heating for optimizing the melting process. For enclosures of high aspect ratios ($A \gtrsim 4$), configurations leading to well controlled heat source temperatures and long melting times are obtained. For cavities of low aspect ratios ($A \lesssim 4$), it is found that the source span η is the most influential parameter. For $\eta \lesssim 0.45$, the melting times are shorter and the heat source temperatures remain equal and moderate during the entire melting process. A map for determining the cavity size and the source distribution that optimizes the melting process is presented.*

Nomenclature

A = cavity aspect ratio (H/W)
a = width of the wall
b = size of the heat sources
c = heat capacity
d = width of the heat sources
e = heat sources span
$\dot{e}_g$ = local generated heat by unit volume ($W \cdot m^{-3}$)
Fo = Fourier number: $\propto_l t/r^2$
F = molten volume fraction
f_ℓ = local liquid fraction
g_i = gravitational acceleration components
H = height of the cavity
h = sensible enthalpy
k = thermal conductivity
L = latent heat of fusion
Nu = Nusselt number: $-(\partial\theta/\partial X)|_w/(\theta_w - \theta_0)$
n = number of heat sources
Pr = Prantdl number: ν/α_ℓ
p = pressure
Q' = total power per unit depth ($W \cdot m^{-1}$)
Ra = Rayleigh number:
r = characteristic length:
SC = subcooling parameter: $c_\ell(T_m - T_0)/L$
Ste = Stefan number:$c_\ell Q'/Lk_\ell$
s = source spacing
T = temperature
t = time
U_i = dimensionless velocity components: u_r/α_ℓ
u_i = velocity components

The authors are very grateful to the Natural Science and Engineering Research Council of Canada (NSERC) and the Fonds pour la Formation de Chercheurs et l'Aide à la Recherche du Québec (FCAR) for their financial support. The authors also thank the Centre de recherches en calcul appliqué of Montréal (CERCA) and the Centre d'applications du calcul parallèle de l'Université de Sherbrooke (CACPUS) for their computer resources.

International Journal of Numerical Methods for Heat & Fluid Flow, Vol. 10 No. 3, 2000, pp. 286-306.

W = half-width of the cavity
X_i = dimensionless coordinates: x_i/r
x_i = Cartesian coordinates

Greek symbols
α = thermal diffusivity
$\bar{\alpha}$ = wall-PCM thermal diffusivity ratio: α_w/α_ℓ
β = dimensionless source size: b/r
β_v = coefficient of volumetric expansion
η = dimensionless source span: e/H
θ = dimensionless temperature: $k_\ell(T - T_m)/Q'$
μ = viscosity
ν = kinematic viscosity
ρ = density
σ = dimensionless spacing: s/r
τ = dimensionless time: Ste·Fo
$\Delta\tau$ = dimensionless time step
τ_{tot} = dimensionless total melting time

Subscripts
ℓ = liquid phase
m = melting point
s = solid phase
s_1, s_2, s_3 = bottom, middle and upper sources
w = wall
0 = initial time

Superscript
* = dimensionless

1. Introduction

This paper presents a numerical study of natural convection dominated melting from discrete heat sources flush mounted on the lateral walls of a rectangular cavity. Our interest for this problem was sparked by the necessity to improve the performance of compact latent heat thermal energy storage systems that have been designed, built and tested in our laboratory (Brousseau and Lacroix, 1996; Millette *et al.,* 1996). These storage units are aimed at smoothing the daily electric load profiles. Their key component consists of a narrow rectangular enclosure, vertically oriented, filled with a phase change material (PCM), for which the lateral vertical walls are covered with equally spaced electric resistance wires. During off-peak hours, usually at night, the heat dissipated by the electric wires is stored as the PCM melts. When the demand for electricity is high, usually the following day, the electric current in the wires is shut off, the PCM resolidifies and the stored heat is recovered.

The problem of melting from discrete heat sources is also relevant to the cooling of electronic components (Peterson and Ortega, 1990). Increasing miniaturization and reduced spacing of chips in an array require larger power dissipation that sometimes cannot be met by conventional passive cooling techniques alone. The use of PCMs is a promising alternative (Pal and Joshi, 1996), particularly well suited for cyclic usage devices.

In both these applications, the natural convection dominated melting in a discretely heated enclosure must be well understood and controlled in order to meet the design and operating conditions. Laboratory experiments conducted for various prototypes revealed that the melting process depends strongly on the cavity aspect ratio and on the distribution of the electric wires. Moreover, difficulties to melt the PCM sitting at the bottom of the cavity and excessive overheating of the PCM and of the top sources are often observed.

In spite of its practical applications, the problem of melting from discrete heat sources has received little attention in the open literature (Pal and Joshi, 1996;

Zhang *et al.,* 1993, 1994; Sasaguchi *et al.,* 1996; Lacroix and Duong, 1998). Moreover, none of the available studies have examined the effects of the cavity dimensions and of the heat source distribution on the melting process. Recently, the authors have presented a computational methodology for predicting the melting process inside uniformly and discretely heated cavities (Binet and Lacroix, 1998). The effect of the source dimensions and span, of the cavity aspect ratio and of the wall-PCM thermal diffusivity ratio was highlighted.

This paper picks up where the previous study has left by shedding new light on the melting process from discrete heat sources and by presenting new results namely:

- laboratory experiments are performed for validating rigorously the numerical model;
- the governing equations are nondimensionalized in such a way that the problem may be entirely defined in terms of four groups of dimensionless parameters;
- the results are generalized for any number of heat sources, all configurations being bounded by two limiting cases;
- the effect of the heat load is investigated; and
- the total melting times are correlated in terms of the source span and cavity aspect ratio.

Also, a new justification is given for the energy source term in Voller's formulation (Voller *et al.,* 1987; Voller and Prakash, 1987; Brent *et al.,* 1988) in the context of convection dominated phase change problems.

2. Physical model and numerical procedure

The physical system considered in the present study is illustrated in Figure 1. An insulated rectangular cavity of width $2W$ is filled with a PCM up to a height H. The space above the PCM is occupied by air. The thickness of the vertical walls is a and their thermal conductivity is k_w. n heat sources of size b

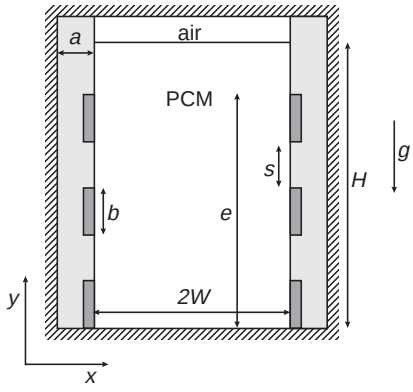

Figure 1.
Schematic representation of the enclosure

separated by a distance s are flush mounted symmetrically on each of the lateral walls. The lowest sources are located at the bottom of the vertical walls. The source span e is defined as $e = nb + (n-1)s$. At time $t < 0$, the discrete heat sources are off. The PCM is solid and the entire system is at a uniform temperature T_0 below the melting point T_m ($T_0 < T_m$). At time $t = 0$, the discrete heat sources are suddenly activated releasing a total of Q' watts per meter of depth on each side wall. As a result, heat is conducted in the walls, transferred to the PCM and melting is eventually triggered.

In formulating the model, the following major assumptions have been made:

- The depth of the cavity (direction perpendicular to the x-y plane, Figure 1) is much larger than the plane dimensions (x-y) so that a two-dimensional analysis can be applied. Also, the fluid motion and heat transfer are symmetrical about the vertical centerline.
- The PCM is pure, homogeneous and isotropic with an isothermal phase change.
- Volumetric expansion is neglected on melting.
- Radiation effects and viscous dissipation are neglected.
- The flow in the liquid phase is laminar, incompressible and Newtonian.
- Buoyancy is taken into account in the momentum equations via the Boussinesq approximation.
- The other thermophysical properties are temperature independent but may be different for the solid and liquid phases.
- The solid PCM is *always* immobilized.

With the foregoing assumptions, the governing equations for the conservation of mass, momentum and energy are:

$$\frac{\partial}{\partial x_i}(\rho u_i) = 0 \tag{1}$$

$$\frac{\partial}{\partial t}(\rho u_i) + \frac{\partial}{\partial x_j}\left(\rho u_j u_i\right) = \mu \frac{\partial^2 u_i}{\partial x_j \partial x_j} - \frac{\partial p}{\partial x_i} - \rho g_i \beta_v (T - T_m) + S_i \tag{2}$$

$$\frac{\partial}{\partial t}(\rho h) + \frac{\partial}{\partial x_j}\left(\rho u_j h\right) = \frac{\partial}{\partial x_j}\left(\frac{k}{c}\frac{\partial}{\partial x_j} h\right) + \dot{e}_g - S_h \tag{3}$$

The volumetric heat sources are provided by the term $\dot{e}_g$ in equation (3). Each source releases Q'/n watts per meter of depth. A symmetry boundary condition is imposed along the vertical centerline and the no slip condition is maintained along the vertical and bottom walls. A full slip boundary condition is applied at the top of the melt.

An overview of the numerical methods for solving phase change problems has recently been published in Voller (1997) and an enthalpy method was

chosen for the present study (Voller *et al.,* 1987; Voller and Prakash, 1987; Brent *et al.,* 1988). This method has been used and validated successfully many times in the past for modeling convection dominated phase change problems (Brent *et al.,* 1988; Ketkar *et al.,* 1991; Viswanath and Jaluria, 1995; Costa *et al.,* 1991; Adetutu and Prasad, 1993; Dantzig, 1987; Lacroix and Voller, 1990).

The energy equation for the PCM follows Voller's formulation (Voller *et al.,* 1987; Voller and Prakash, 1987; Brent *et al.,* 1988) for which the total energy is split into sensible and latent heat components:

$$H(T) = h(T) + Lf_\ell \tag{4}$$

where

$$h(T) = \int_{T_m}^{T} cdT \tag{5}$$

and f_ℓ is the local liquid fraction. The advantage of this formulation is that the enthalpy equation for the PCM and for the wall is cast in a standard form and the complexity associated with the phase change is isolated in the source term S_h. Then, it is easy to show (Voller *et al.,* 1987; Voller and Prakash, 1987) that this source term is given by:

$$S_h = \rho L \frac{\partial f_\ell}{\partial t} + \rho L \frac{\partial}{\partial x_i}(u_i f_\ell) \tag{6}$$

The convective part of S_h (second term) vanishes when the phase change is isothermal. The relation between f_ℓ and h is then given by the Heaviside step function:

$$f_\ell = \begin{cases} 1 & \text{if } h > 0 \\ 0 & \text{if } h < 0 \end{cases} \tag{7}$$

and this convective term can be split in two parts:

$$\rho L \frac{\partial}{\partial x_i}(u_i f_\ell) = \rho L f_\ell \frac{\partial u_i}{\partial x_i} + \rho L u_i \frac{\partial f_\ell}{\partial x_i} \tag{8}$$

The first term of the right hand side of equation (8) cancels out for an incompressible flow. The second term vanishes in regions where f_ℓ is uniform, but it is indeterminate at the melting front where the derivative $\partial f_\ell / \partial x_i$ goes to infinity. It is possible, however, to rewrite this term in a coordinate system $(\bar{x}, \bar{y})$ for which the vertical axis lies along the phase front. In this case,

$$\begin{aligned} \rho L u_i \frac{\partial f_\ell}{\partial x_i} &= \rho L u(\bar{x}) \frac{d}{d\bar{x}} f_\ell(\bar{x}) \\ &= \rho L u(\bar{x}) \delta(\bar{x}) \end{aligned} \tag{9}$$

where $\delta(\bar{x})$ is defined as the Dirac delta function. It is equal to zero everywhere in the calculation domain except at the origin, i.e. the phase front, where it becomes infinite. However, for a function $g(\bar{x})$ equal to zero at the origin, the following property is satisfied (Butkov, 1968):

$$g(\bar{x})\delta(\bar{x}) = 0 \text{ if } g(0) = 0 \tag{10}$$

Since the no slip boundary condition is valid at the phase front (the melting front velocity is much smaller than the buoyancy driven melt velocity), i.e. $u(0) = 0$, then:

$$\rho L u_i \frac{\partial f_\ell}{\partial x_i} = 0 \tag{11}$$

Of course, the liquid fraction f_ℓ is fixed to zero inside the walls and, as a result, $S_h = 0$.

The liquid fraction is also used to drive the velocity components to zero in the solid phase of the PCM and in the solid walls of the cavity via the source terms S_i in the momentum equations (2):

$$S_i = -B(f_\ell)u_i \tag{12}$$

The function B becomes very large when f_ℓ is zero and goes to zero as f_ℓ tends to one. A function B based on the Carman-Kozeny relation for a porous medium, as described in Voller *et al.* (1987), Voller and Prakash (1987) and Brent *et al.* (1988), was employed in this study:

$$B(f_\ell) = \frac{C(1 - f_\ell)^2}{(f_\ell^3 + \varepsilon)} \tag{13}$$

with $C = 1.6 \times 10^6$ and $\varepsilon = 1.0 \times 10^{-3}$. When compared with other techniques for switching off the velocities (Voller *et al.,* 1987), this numerical artifact is relatively stable. It may also be seen as a convenient way for modeling the transition zone between the solid and liquid phases.

The finite difference equations are obtained on integrating the conservation equations (1)-(3) over each of the control volumes in the (x,y) plane using second-order centered differences. To avoid numerical instability, the advection terms are discretized with a hybrid difference scheme (Spalding, 1972). Simulations were also conducted for higher order difference schemes. When convergence was successfully attained, at the expense of significantly longer calculation times, the results for the location of the solid-liquid interface, heat source temperatures and Nusselt numbers did not show noticeable differences with those obtained with the hybrid scheme. The convection coefficients are obtained from the Rhie and Chow interpolation formula (Rhie, 1981). With this scheme, all the variables are located on a non-staggered grid. An implicit Euler scheme is used for the time-stepping procedure. The SIMPLEC algorithm (Van Doormal and Raithby, 1984) is adopted for the

velocity-pressure coupling. The set of linearized equations is solved iteratively with a line-by-line tridiagonal matrix algorithm (TDMA) solver by sweeping the cavity from left to right. Further details on the numerical scheme are reported in Binet and Lacroix (1998) and need not be repeated here.

3. Experimental set-up and validation

The above computational model has been successfully employed to simulate various phase change problems. First, it has been confronted to the Neumann solution for the case of one-dimensional solidification by conduction (Carslaw and Jaeger, 1959). Second, the model has been tested and validated with experimental (Gau and Viskanta, 1986) and numerical (Brent *et al.,* 1988) data for the natural convection dominated melting of gallium (Pr = 0.0216) from an isothermal vertical wall. Third, it has been compared to the experimental data of Zhang *et al.* (1993) for the melting of octadecane (Pr = 53.5) in a discretely heated enclosure. The results of this validation are reported elsewhere (Binet and Lacroix, 1998). Finally, it has been validated with experimental data obtained in our laboratory. This is the subject of the present discussion.

A layout of the experimental test section is shown in Figure 2. The enclosure has inside dimensions of 19cm in height, 2cm in width and 40cm in length and is filled with a PCM. The top, bottom, front and side walls are made of Plexiglas which allows visualization of the melt. The thickness of the top, bottom and side walls is 0.9cm. The front wall is 1.2cm thick. Electric wires (1.54 (Ω/m) made out of nickel-chrome are glued to the left inner side wall to the desired vertical locations and are displayed horizontally so that two-dimensional melting around the heat sources is promoted. The test cell is supported by a

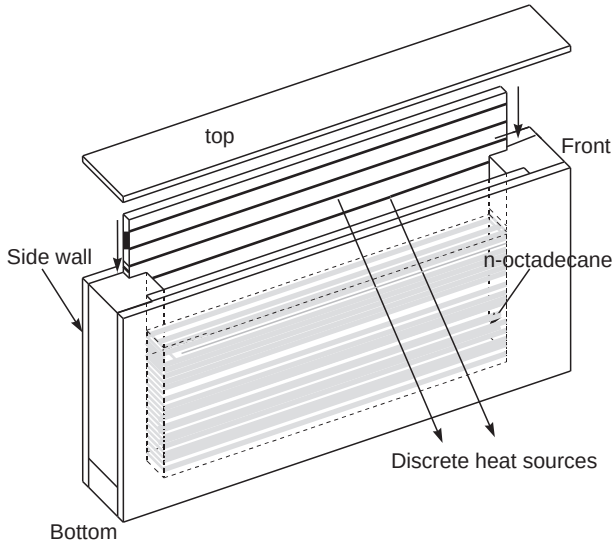

Figure 2.
Schematic respresentation of the vertical test section

wooden frame and it is well insulated with fiberglass wool and air gaps. For the front wall, the insulation is mounted on a panel which can be removed to take snapshots during the melting process.

The entire experimental set-up is depicted in Figure 3. A power supply controls the electric power dissipated in the heaters. The temperature of the heaters is measured by means of constantan-copper thermocouples (type T) connected to a data acquisition system (16 channels multiplexer-amplifiers and 8 channels 12 bits A/D converter). The thermocouples were calibrated using a temperature controlled heating bath and a standard thermometer. The accuracy of the temperature measurements is $\pm$ 0.75K. The temperatures are recorded at one minute intervals during the melting process. The solid-liquid profiles are photographed with a computer camera EDC-1000 and the contours are digitized with a computer. Further details on the experimental set-up are provided in Lacroix and Duong (1998).

Research grade (99 per cent pure) octadecane is used as the PCM. When molten, it is transparent to visible light, thus allowing for photographic observation of the melt zone. Its melting temperature is near the ambient (28°C) which minimizes the heat losses/gains to the surroundings. Its thermophysical properties are also relatively well established (Table I) (Daubert and Danner, 1989). The filling of the enclosure with liquid PCM is critical due the possibilities of entrapping air bubbles. Therefore, the pouring of octadecane into the enclosure is limited to a small amount (1cm deep layer) at a time. Once the layer is solidified, the next layer is added.

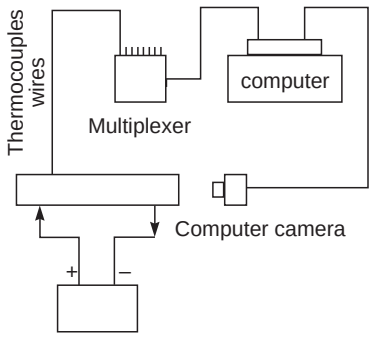

Figure 3.
Schematic diagram of the experimental set-up

c_ℓ	2.231	T_m	301.33
c_s	1.891	β	$9.1X10^{-4}$
k_ℓ	0.150	μ	$3.6X10^{-3}$
k_s	0.380	ρ	771.2
L	243 477		

Table I.
Thermophysical properties of octadecane

For the present validation case, two heat sources of dimension b = 1.1cm were mounted on the left vertical side wall at 2.3 and 4.8cm from the bottom of the enclosure. The total electric power dissipated by unit length Q' is 50W/m. The initial temperature of the solid PCM was T_o = 295K.

An area of 2cm in width and 9.5 cm in height was mapped with 40X76 uniformly distributed control volumes to numerically simulate the melting process. Time steps of 7.5 s for the first 20 minutes of simulation and 15 s afterwards were employed to conduct the calculations. Numerical simulations performed with finer grids and smaller time steps did not show perceptible differences with the present results.

Figure 4 shows a comparison of the predicted solid-liquid interface positions with those determined experimentally. The agreement between the numerical results and the experimental data is good. The slight shift between the predicted and measured interface positions is mainly due to the limitations of the model (two-dimensional model) and also to the difficulties of maintaining a constant heat generation output from the heaters in the course of the experiment.

The corresponding time wise variation of the predicted and measured temperatures are depicted in Figure 5 for both heat sources. Again, except for the first few minutes of the transient, the agreement between the predictions and the data is within the experimental uncertainties. Further details on the validation of the present model are provided in Binet and Lacroix (1998) and Binet (1998).

4. Parametric study

A series of numerical simulations was conducted to determine the effect of the number of heat sources n, of their size β and span η and of the cavity aspect

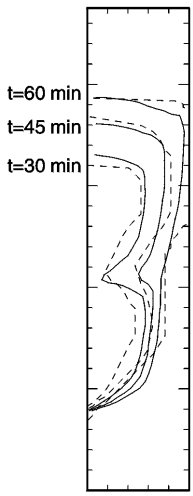

Figure 4.
Melting front positions: predictions (solid lines); data (dashed lines)

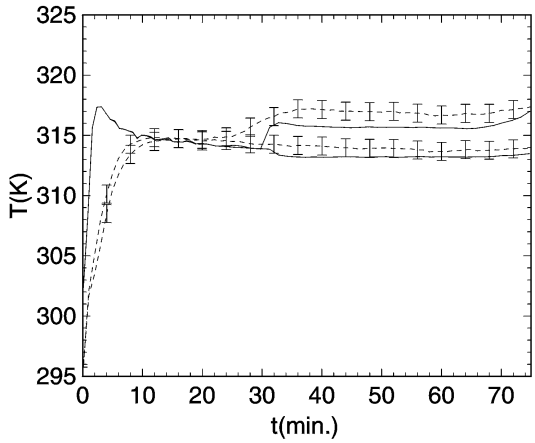

Figure 5.
Temperature evolution: predictions (solid lines); data (dashed lines)

ratio $A = H/W$ on the melting process. The effect of the wall thermal diffusivity has been reported in Zhang *et al.* (1994), Binet and Lacroix (1998) and Zhang and Chen (1994) and will not be discussed here.

The main objective of the present study is to optimize the melting of a fixed amount of PCM provided that the heat load Q' remains constant. By optimization, we mean, first, to maintain the temperature of the sources as low as possible and, second, "for heat storage", to minimize the melting time or "for the cooling of heat sources", to prolong as much as possible the melting period. It must be pointed out that all simulations were carried out until the PCM in the cavity was entirely melted. As a result, the melting time is problem dependent and the total energy supplied (in joules) may vary from one simulation to another, even though the heat load Q' (W/m) remains the same.

For the purpose of the discussion, the governing equations (1)-(3) were nondimensionalized in the following manner:

$$\frac{\partial U_i}{\partial X_i} = 0 \tag{14}$$

$$\frac{\partial U_i}{\partial Fo} + \frac{\partial (U_j U_i)}{\partial X_j} = \Pr \frac{\partial^2 U_i}{\partial X_j \partial X_j} - \frac{\partial p^*}{\partial X_i} - Ra \Pr \frac{g_i}{|\vec{g}|}\theta - B^* U_i \tag{15}$$

$$\frac{\partial \theta}{\partial Fo} + \frac{\partial (U_j \theta)}{\partial X_j} = \frac{\partial}{\partial X_j}\left(\alpha^* \frac{\partial \theta}{\partial X_j}\right) - \frac{1}{\mathrm{Ste}} \frac{\partial f_\ell}{\partial \mathrm{Fo}} + \dot{E}_g \tag{16}$$

$$\left.\begin{matrix} Y = 0 \\ Y = \sqrt{A} \end{matrix}\right\} \Rightarrow \frac{\partial \theta}{\partial Y} = 0 \left.\begin{matrix} X = \frac{1}{\sqrt{A}} \\ X = -a^* \end{matrix}\right\} \Rightarrow \frac{\partial \theta}{\partial X} = 0 \tag{17}$$

$$\theta_0 = -\frac{SC}{\mathrm{Ste}} \tag{18}$$

where

$$\alpha^* = \begin{cases} \bar{\alpha} & \text{in the wall} \\ f_\ell + (1 - f_\ell)\dfrac{\alpha_s}{\alpha_\ell} & \text{in the PCM} \end{cases} \tag{19}$$

$$\dot{E}_g = \begin{cases} \dfrac{1}{n\beta d^*} & \text{for a segment occupied by a source} \\ 0 & \text{elsewhere} \end{cases} \tag{20}$$

The length scale r is defined as $\sqrt{HW}$ and the temperature scale is taken as Q'/k_ℓ. These scales remain invariant as long as the mass of PCM and the heat load are kept constant. Consequently, the Rayleigh (Ra) and Stefan (Ste) numbers are not functions of the imposed heat flux as reported in most studies devoted to natural convection from discrete heat flux sources (Chadwick *et al.,* 1991; Ho and Chang, 1994; Refai and Yovanovich, 1990). Ra and Ste remain unchanged even if the aspect ratio of the cavity and/or the source configuration is modified.

The dimensionless time τ = Ste·Fo provides a measuring stick for the total amount of energy released by the heat sources. A value of unity corresponds to the time needed to melt entirely the PCM with no subcooling and no sensible heat storage. The dimensionless temperature Ste·θ reflects the local excess of sensible heat with respect to latent heat. A value of unity means that there is as much sensible heat as latent heat stored at that particular control volume and it translates into excessive temperature (approx. 110K above the melting point of octadecane). Of course, at the phase front, Ste·θ = 0.

The source span η is nondimensionalized with respect to the height of the cavity H. For η = 1, the clearance between the sources along the lateral wall is maximum and for η = 0, the sources are all gathered in a single point at the bottom. The relation between the source span η and their number n, their size β and their spacing σ is given by:

$$\eta = \frac{(n\beta + (n-1)\sigma)}{\sqrt{A}} \tag{21}$$

β and η are the two independent parameters chosen here. When the number n and the size β are fixed, the total power dissipated by each source is constant even if the cavity aspect ratio is modified. This ensures that the heat source distribution remains independent of the cavity dimensions.

The problem is now completely defined by four dimensionless groups for the material properties, the cavity geometry, the source configuration and the melting/flow dynamics. These dimensionless groups are provided in Table II. If not specified otherwise, the parameters are assigned to the values indicated

by a star (*). As will be seen in the next section, the present way of nondimensionalizing the conservation equations will shed some interesting and practical observations on the results.

All calculations were conducted with meshes stretching from 20X160 to 100X30 uniformly distributed control volumes in the PCM. Moreover, grids of 10X160 to 10X30 uniformly distributed control volumes were employed to model heat conduction in the vertical side wall. Time steps $\Delta\tau$ ranging from $6.81X10^{-4}$ to $2.73X10^{-3}$ were used for the study. Once again, simulations were carried out with finer meshes and smaller time steps in order to check the accuracy of the predictions. In all cases, they did not show perceptible differences with the present results. Typical CPU times on an IBM RS/6000 model 375 ranged from 12h to 24h, depending on the simulated scenario.

5. Results and discussion

Two general observations may readily be made for cavities of high aspect ratio ($A \gtrsim 4$). First, if the heat sources are spread apart, the numerical model predicts that lumps of solid PCM may remain suspended along the symmetry axis between the sources (Figure 6a). Since, for most PCMs, the density of the solid phase is larger than that of the liquid phase, these lumps will sink at the bottom of the cavity thereby pushing the melt upwards. Even though the present model cannot predict such an event, it leads to a situation where the heat released by the upper sources contributes more to the overheating of the melt than to the melting of the PCM. The net result is a decrease of the melting rate. Only some particular cases do not behave this way (Binet and Lacroix, 1998).

Second, it is observed, for heat sources closely spaced near the bottom of the enclosure, that the solid-liquid interface quickly becomes horizontal and heat is transferred from the melt to the solid through a minimal surface (Figure 6b). As a result, the melting rate is slowed down. This behavior has also been observed experimentally (Lacroix and Duong, 1998). For this case, the temperature of the heat sources is well under control as solid PCM lies above them for the entire duration of the melting process (Binet and Lacroix, 1998).

When the aspect ratio is reduced to $A \lesssim 4$, the cavity is wide enough so that the solid-liquid interface never becomes horizontal. Furthermore, for widely spaced heat sources, the problem of sinking PCM is not likely to arise. Figure 7 elucidates the effect of the number of heat sources n and of their span η and size β on the melting time for three such enclosures and two different electric heat loads (Ra and Ste). It is clear from this figure that the melting time is chiefly dominated by the source span η and its effect is accentuated for larger aspect

α_s/α_ℓ	2.53	A	0.1 to 40
Pr	57.3	β	0.0316 to 0.158
SC	$5.18X10^{-2}$	η	0.075 to 1.0
d*	0.0316	n	1, 3 and 9
a*	0.316	Ra	$1.77X10^{8}$* and $2.94X10^{7}$
$\bar{\alpha}$	1.50	Ste	1.82* and 0.30

Table II. Dimensionless parameters

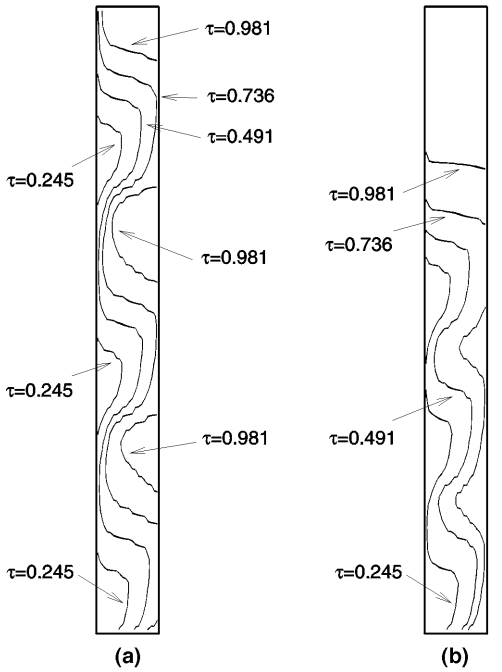

Figure 6.
Melting front positions for $A = 10$, $n = 3$, $\beta = 0.158$: (a) $\eta = 0.775$; (b) $\eta = 0.55$

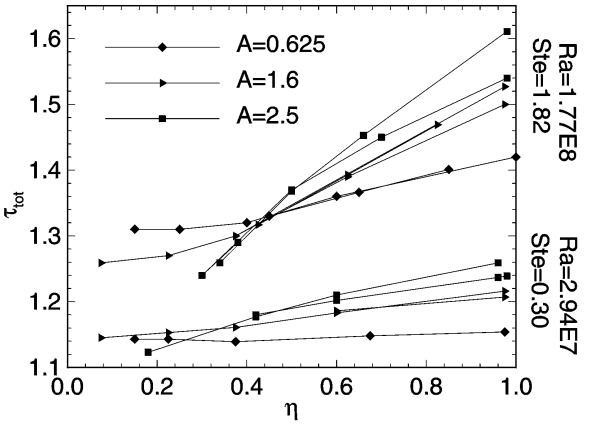

Figure 7.
Effect of the sources span and size on the melting time

ratios and larger electric heat loads. Consequently, the source span or the *total heated length* (Bejan, 1996) appears to be the main parameter characterizing the source distribution. Also, Figure 7 shows that the potential reduction for the melting time (by reducing the span) increases for higher aspect ratios and/or stronger electric heat loads.

For $\eta \gtrsim 0.5$, the melting time becomes a multivalue function bounded by two limits (Figure 8). The upper limit corresponds to a uniformly heated section ($n = 1$) of length η. This limit is also reached as the number of heat sources increases. In this case, the source spacing becomes so small ($\sigma \rightarrow 0$) that the

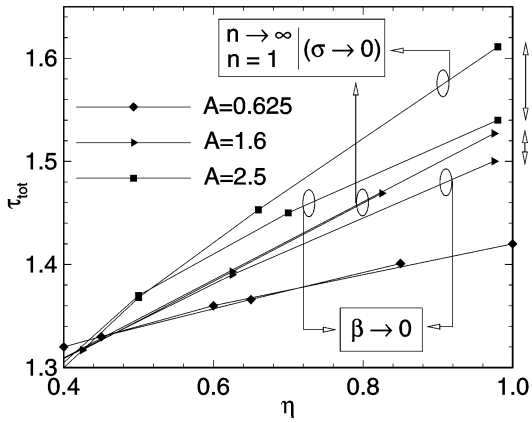

Figure 8.
Effect of the source distribution on the melting time (zoomed area)

effect of discrete heating can no longer be distinguished from that of uniform heating. For instance, for a cavity of aspect ratio $A = 2.5$, the distinct effect of discrete heating vanishes for $\beta = 0.0316$ and $n = 9$. Therefore, it is not necessary for the present study to perform simulations for a larger number of heat sources. On the other hand, the lower limit corresponds to a line heat source distribution ($\beta \rightarrow 0$). In this case, the number of heat sources is small, and so is their size, and the effect of discrete heating is emphasized. For example, for $A = 1.6$, the lower limit is reached with $\beta = 0.158$ and $n = 3$. All the simulations reported here fall between the upper and the lower limit. As η diminishes, to two limits merge and the heating effect becomes similar to that of a single heat source. Again, this multivalue effect increases with A and Ra (Ste).

To illustrate the benefits of discrete heating for accelerating the melting process, two limiting test cases were scrutinized (Figure 9). For both cases, $A = 2.5$ and $\eta = 0.98$ (largest gap on Figure 8). For case (a), the upper limit, the number of heat sources n is set equal to 9 and their dimension β is 0.0316. For case (b), the lower limit, the number of heat sources n is set equal to 3 and their size remains the same, i.e. $\beta = 0.0316$. Figure 9 shows that the time evolution of the velocity vector fields for case (a) is similar to that for a uniformly heated wall: early in the process, a single recirculation zone appears in the liquid phase, grows in size and melting is enhanced at the top. For case (b) the melting process is clearly different. Melt zones grow separately around each source and merge eventually. It is evident, in this case, that the heat transferred from the bottom heat source maintains vigorous buoyancy driven flows in the lower part of the cavity thereby accelerating the melting process in this critical region. Sasaguchi *et al.* (1996) have also observed this behavior. Melting is faster with multiple recirculation zones triggered from discrete heat sources.

The corresponding local Nusselt numbers at the wall/PCM interface for both cases at time $\tau = 0.491$ and time $\tau = 0.981$ are depicted in Figure 10 and Figure 11 respectively. At early times (time $\tau = 0.491$), the Nusselt number in the vicinity of the three sources (case b) is obviously larger than that of the nine

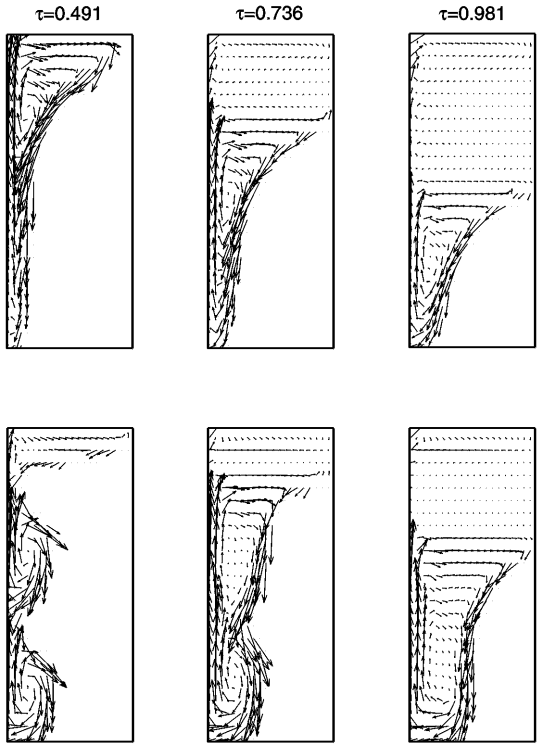

Figure 9.
Time evolution of the velocity fiels for $A = 2.5$, $\eta = 0.98$ and $\beta = 0.0316$: $n = 9$ (top); $n = 3$ (bottom)

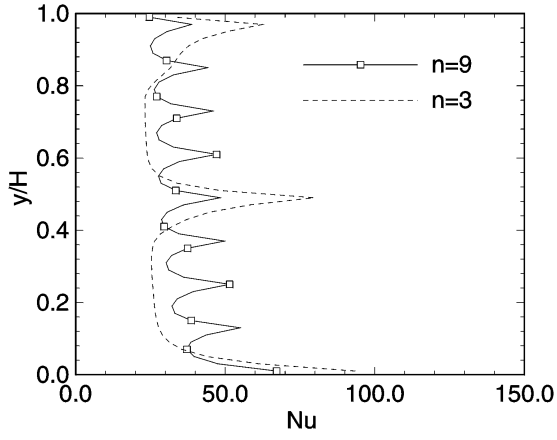

Figure 10.
Local Nusselt number at τ 0.491 for $A = 2.5$, $\eta = 0.98$ and $\beta = 0.0316$

sources (case a) since the input heat flux is larger in the former than in the latter. However, at the time $\tau = 0.981$, the Nusselt number for the three sources exceeds that for the nine sources on the entire surface of the wall, as vigorous buoyancy driven flows prevail in most of the melt.

The effect of the source span η is now discussed. Figure 12 illustrates the time-varying heat source temperature and interface position for a case where

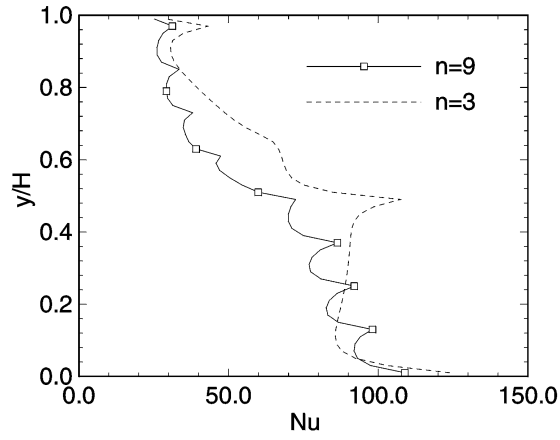

Figure 11.
Local Nusselt number at $\tau = 0.981$ for $A = 2.5$, $\eta = 0.98$ and $\beta = 0.0316$

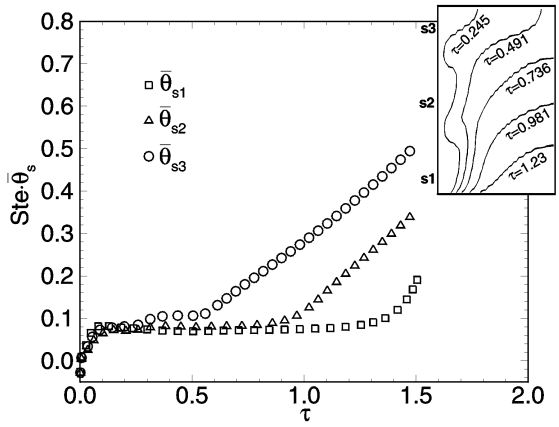

Figure 12.
Average surface temperature of discrete heat sources and phase front shapes for $A = 1.6$, $n = 3$, β 0.158 and $\eta = 0.975$

the heat sources are spread apart ($\eta = 0.975$). As time passes, the phase front progresses from left to right and becomes increasingly bent. As a result, at time $\tau = 1.23$, a solid block of PCM still sits at the bottom of the cavity while the top sources are dangerously overheating. Such a situation is undesirable for the cooling of electronic components or for the operation of latent heat thermal energy storage systems as mentioned in the introduction. The sudden rise in the temperature of the sources (break of the quasi-steady regime) corresponds to the time when the solid-liquid interface reaches the middle vertical plane of the cavity at the level of the corresponding heat source. However, gathering the sources at the bottom of the lateral walls ($\eta = 0.375$) maintains the same temperature for all sources and prevents overheating of the top ones while the PCM is still melting (Figure 13). In this case, it is seen that the solid-liquid interface remains mostly vertical as it recedes from the heat sources thereby promoting a more uniform melting of the solid PCM.

The total melting time of the cases shown in Figure 7 was correlated for the source span η and the cavity aspect ratio A. The results, depicted as a three

dimensional plot in Figure 14, were correlated with a least square fit by the following equation:

$$\tau(\eta, A) = C_1 + C_2 \ln(\eta) + C_3 A + C_4 (\ln(\eta))^2 + C_5 A^2 + C_6 \ln(\eta) A \qquad (22)$$

The constants C_1-C_6 are provided in Table III for the two limits ($n \to \infty$ and $\beta \to 0$) and two different power inputs. Interestingly enough, when $\eta \to 1$, the above correlation becomes:

$$\tau(1, A) = C_1 + C_3 A + C_5 A^2 \qquad (23)$$

The estimated standard deviation for this correlation is $8.1\text{X}10^{-3}$.

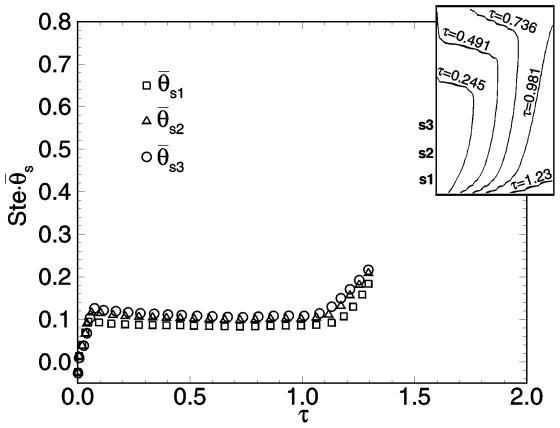

Figure 13.
Average surface temperature of discrete heat sources and phase front shapes for $A = 1.6$, $n = 3$, $\beta = 0.158$ and $\eta = 0.375$

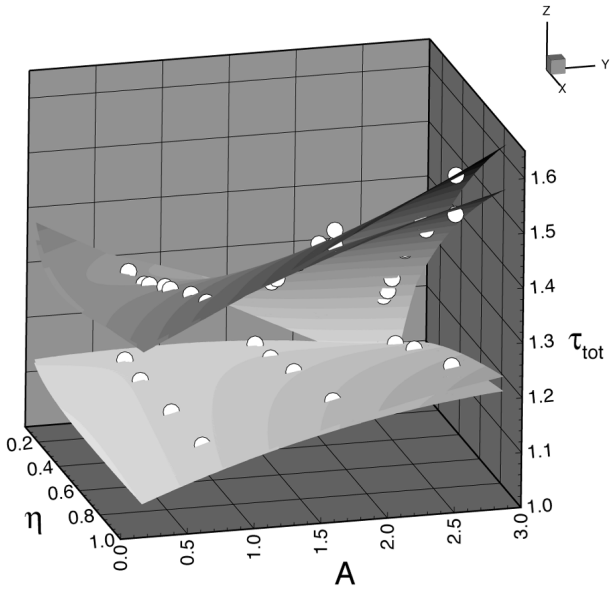

Figure 14.
Effect of the distribution span and enclosure aspect ratio on the melting time (correlation)

It may also be observed from Figure 7 that unlike the case of a constant temperature wall (Gau and Viskanta, 1986), melting from heat sources is more efficient when the electric power is reduced. Indeed, the wall temperature is nonuniform and time dependent and the role of sensible heat storage is significant. For the test cases examined in the present study, the wall and PCM thermal diffusivities are comparably small and reducing the power input to the sources allows time (in seconds) for heat to diffuse through these materials, thereby avoiding overheating and yielding more efficient melting. Figure 15 illustrates such a behavior by comparing the time varying solid-liquid interface positions for two different power inputs. The corresponding temporal variation of the molten volume fraction is depicted in Figure 16. Clearly, the melting process lags behind (dimensionless time) when the power input is larger. This lag starts to appear when the solid-liquid interface reaches the middle vertical plane of the cavity ($\tau \approx 0.5$) i.e. when overheating is experienced. This explains why the effect of heat load is stronger when the heat source span η is larger (Figure 7), i.e. when the sources are more likely to overheat.

The overall effect of the cavity aspect ratio and of the heat source distribution is summarized in Figure 17 in terms of the maximum heat source temperature and of the total melting time. The number n and size β of the heat sources are kept constant at 3 and 0.158, respectively. Two simulations conducted with a uniformly heated non conducting wall are also shown (Binet

	Ra = 1.77 $\times 10^8$ (Ste = 1.82) upper limit	Ra = 1.77 $\times 10^8$ (Ste = 1.82) lower limit	Ra = 2.94 $\times 10^7$ (Ste = 0.30) upper limit	Ra = 2.94 $\times 10^7$ (Ste = 0.30) lower limit
C_1	1.36676	1.37062	1.10635	1.10581
C_2	0.0921470	0.121628	0.0132260	0.00952359
C_3	0.0924945	0.0951486	0.0871163	0.0875960
C_4	0.0568477	0.0622336	0.0173946	0.0132594
C_5	0.00252142	–0.00863437	–0.0102100	–0.0134194
C_6	0.118461	0.0839465	0.0382476	0.0320836

Table III.
Correlation coefficients

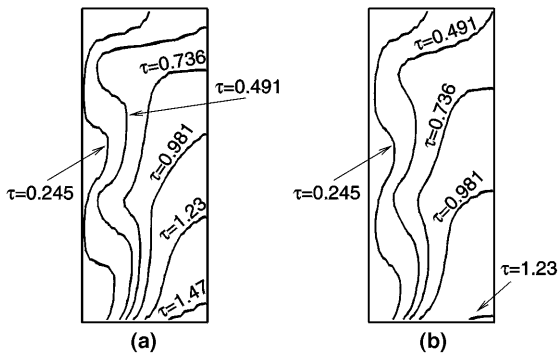

Figure 15.
Melting front shapes for A = 2.5, n = 3, η 0.98 and β = 0.0316: (a) Ra = 1.77E8 and Ste = 1.82; (b) Ra = 2.94E7 and Ste = 0.30

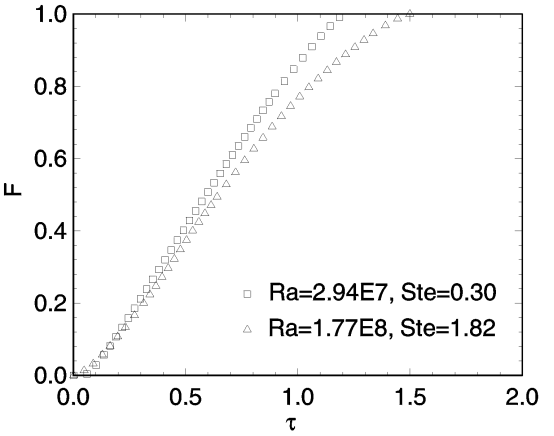

Figure 16.
Time evolution of the molten volume fraction for A = 2.5, n = 3, η = 0.98 and β = 0.0316

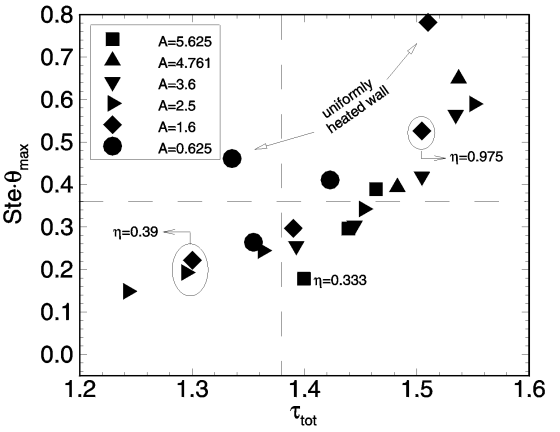

Figure 17.
Melting times and maximum source temperature for various configurations

and Lacroix, 1998). An overview of this figure reveals the benefits of discrete heating. Configurations in the lower left quadrant are well suited for heat storage applications (short melting periods and small source temperatures) while those in the lower right quadrant are recommended for the cooling of electronic components (long melting periods and small source temperatures).

6. Conclusion

A numerical study was conducted for natural convection dominated melting inside discretely heated rectangular enclosures. Results have shown the indisputable benefits of discrete heating over uniform heating for optimizing the melting process. For enclosures of high aspect ratios ($A \gtrsim 4$), configurations leading to well controlled heat source temperatures and long melting times have been obtained. It was found, on the other hand, that for cavities of lower aspect ratio ($A \lesssim 4$) the source span η is the most influential parameter on the melting time. All source configurations are bounded by two limits: a lower limit corresponding to a line heat source distribution ($\beta \rightarrow 0$) and an upper limit

corresponding to a uniformly heated wall section. Both these limits merge for a source span $\eta \lesssim 0.5$. For $0.625 \lesssim A \lesssim 2.5$ and $\eta \gtrsim 0.45$, the melting times are longer and the top sources quickly overheat. If $\eta \gtrsim 0.45$, the melting times are shorter and the heat source temperatures remain equal and moderate during the entire melting process. Melting from heat sources is more efficient when the electric power is reduced.

References

Adetutu, O. and Prasad, V. (1993), "Melting in rectangular and cylindrical cavities: effect of curvature, aspect ratio and buoyancy forces", *Advanced Computations in Materials Processing*, ASME HTD, Vol. 241.

Bejan, A. (1996), "Geometric optimization of cooling techniques", in Kim, S.J. and Lee, S.W. (Eds), *Air Cooling Technology for Electronic Equipment*, CRC Press, Boca Raton, FL.

Binet, B. (1998), "Étude de la fusion dans des enceintes munies de sources de chaleur discrètes", PhD thesis, dept. of mechanical engineering, Université de Sherbrooke, Québec.

Binet, B. and Lacroix, M. (1998), "Étude numérique de la fusion dans des enceintes rectangulaires chauffées uniformément ou discrètement par les parois latérales conductrices", *Revue Générale de Thermique*, Vol. 37, pp. 607-20.

Brent, A.D., Voller, V.R. and Reid, K.J. (1988), "Enthalpy – porosity technique for modeling convection-diffusion phase change: application to the melting of a pure metal", *Numerical Heat Transfer*, Vol. 13, pp. 297-318.

Brousseau, P. and Lacroix, M. (1996), "Study of the thermal performance of a multi-layer PCM storage unit", *J. of Energy Conversion and Management*, Vol. 37, pp. 599-609.

Butkov, E. (1968), *Mathematical Physics*, Addison-Wesley, Reading, MA.

Carslaw, H.S. and Jaeger, J.C. (1959), *Conduction of Heat in Solids*, 2nd ed., Clarendon Press, Oxford.

Chadwick, M.L., Webb, B.W. and Heaton, H.S. (1991), "Natural convection from two-dimensional discrete heat sources in a rectangular enclosure", *Int. J. Heat Mass Transfer*, Vol. 34, pp. 1679-93.

Costa, M., Oliva, A., Segarra, C.D.P. and Alba, R. (1991), "Numerical simulation of solid-liquid phase change phenomena", *Comput. Methods Appl. Mech. Engrg.*, Vol. 91, pp. 1123-34.

Dantzig, J.A. (1987), "Modelling liquid-solid phase changes with melt convection", *Int. J. for Num. Meth. Engng*, Vol. 28, pp. 1768-85.

Daubert, T.E. and Danner, R.P. (1989), "Physical and thermodynamic properties of pure chemicals: data compilation", *Hemisphere*.

Gau, C. and Viskanta, R. (1986), "Melting and solidification of a pure metal on a vertical wall", *J. Heat Transfer*, Vol. 108, pp. 174-81.

Ho, C.J. and Chang, J.Y. (1994), "A study of natural convection heat transfer in a vertical rectangular enclosure with two-dimensional discrete heating: effect of aspect ratio", *Int. J. Heat Mass Transfer*, Vol. 37, pp. 917-25.

Ketkar, S.P., Parang, M. and Arimilli, R.V. (1991), "Experimental and numerical study of solidification and melting of pure materials", *J. Thermophysics*, Vol. 5, pp. 40-5.

Lacroix, M. and Duong, T. (1998), "Experimental improvements of heat transfer in a latent heat thermal energy storage unit with embedded heat sources", *J. of Energy Conversion and Management*, Vol. 39, pp. 703-16.

Lacroix, M. and Voller, V.R. (1990), "Finite difference solutions of solidification phase change problems: transformed versus fixed grids", *Numerical Heat Transfer Part B*, Vol. 17, pp. 25-41.

Millette, J., Lacroix, M. and Galanis, N. (1996), "Design, building and testing of a latent heat thermal energy storage element", *Fifth International Symposium on Thermal Engineering and Science for Cold Regions*, Ottawa.

Pal, D. and Joshi, Y. (1996), "Application of phase change materials for passive thermal control of plastic quad flat packages: a computational study", *Numerical Heat Transfer Part A*, Vol. 30, pp. 19-34.

Peterson, G.P. and Ortega, A. (1990), "Thermal control of electronic equipment and devices", in *Advances in Heat Transfer*, Vol. 20, Academic Press, New York, NY.

Refai, G. and Yovanovich, M.M. (1990), "Influence of discrete heat source location on natural convection heat transfer in a vertical square enclosure", *General Papers: Phase Change and Convective Heat Transfer, Presented at AIAA/ASME Thermophysics and Heat Transfer Conference*, June 18-20, 1990, Seattle, Washington, ASME HTD, Vol. 129, 1990.

Rhie, C.M. (1981), "A numerical study of the flow past an isolated airfoil with separation", PhD thesis, Dept. of Mechanical and Industrial Engineering, University of Illinois at Urbana-Champaign, IL.

Sasaguchi, K., Ishihara, A. and Zhang, H. (1996), "Numerical study on utilization of melting of phase change material for cooling of a heated surface at a constant rate", *Numerical Heat Transfer Part A*, Vol. 29, pp. 19-31.

Spalding, D.B. (1972), "A novel finite difference formulation for differential expressions involving both first and second derivatives", *Int. J. for Num. Meth. Engng*, Vol. 4, pp. 551-9.

Van Doormal, J.P. and Raithby, G.D. (1984), "Enhancements of the SIMPLE method for predicting incompressible fluid flows", *Numerical Heat Transfer*, Vol. 7, pp. 147-63.

Viswanath, R. and Jaluria, Y. (1995), "Numerical study of conjugate transient solidification in an enclosed region", *Numerical Heat Transfer Part A*, Vol. 27, pp. 519-36.

Voller, V.R. (1997), "An overview of numerical methods for solving phase change problems", in Minkowycz, W.J. and Sparrow, E.M. (Eds), *Advances in Numerical Heat Transfer*, Vol. 1, Taylor & Francis, Basingstoke.

Voller, V.R. and Prakash, C. (1987), "A fixed grid numerical modelling methodology for convection-diffusion mushy region phase-change problems", *Int. J. Heat Mass Transfer*, Vol. 30 No. 8, pp. 1709-19.

Voller, V.R., Cross, M. and Markatos, N.C. (1987), "An enthalpy method for convection/diffusion phase change", *Int. J. for Num. Meth. Engng*, Vol. 24, pp. 271-84.

Zhang, Y. and Chen, Z. (1994), "Effect of wall conduction on melting in an enclosure heated at constant rate", *Int. J. Heat Mass Transfer*, Vol. 37, pp. 340-3.

Zhang, Y., Chen, Z. and Wang, Q. (1994), "Analysis of melting in an enclosure with discrete heating at constant rate", *Int. J. Heat and Fluid Flow*, Vol. 15, pp. 79-82.

Zhang, Y., Chen, Z., Wang, Q. and Wu, Q. (1993), "Melting in an enclosure with discrete heating at constant rate", *Experimental Thermal and Fluid Science*, Vol. 6, pp. 196-201.